Evaluation of Novel Airborne Gravity Levelling Methods

Felix Johann, Hannes Eisermann, Antonia Ruppel, and Graeme Eagles

Abstract

In dynamic gravimetry, i.e. airborne and shipborne gravimetry, levelling methods are used to refine gravity disturbance results based on neighbouring trajectories. In the traditional crossover adjustment, line biases are estimated using gravity disturbance residuals at trajectory line crossings as input to a least-squares adjustment. In an alternative method, the results along the complete trajectory are used to estimate the gravity disturbance field in the survey area and line biases in a one-step least-squares adjustment applying spherical radial basis functions. This makes the bias estimation more robust since the observations are not restricted to a small number of residuals at crossings strongly affected by random errors. Adjustment becomes applicable to a wider range of campaigns including irregular trajectories without many crossings. Within the scope of this work, existing methods that estimate line biases are extended to bias estimation based on trajectory segments with inter-bias interpolation. The extended method can be particularly useful for irregular trajectories without a sufficient number of line crossings. The introduced levelling methods are evaluated at the example of three airborne campaigns: a fixed wing survey at Germany with a very dense grid, a fixed wing survey in East Antarctica with varying line separation, and a helicopter survey on Svalbard with highly irregular trajectories. It is shown that the levelling method based on spherical radial basis functions improves the precision in all evaluated campaigns, even when a traditional crossover levelling is not possible.

Keywords

Adjustment · Airborne gravimetry · Levelling · Radial basis functions · Strapdown

1 Introduction

In dynamic gravimetry, the gravity field is observed from a moving platform like an aircraft (airborne gravimetry) or a ship (shipborne gravimetry). In contrast to highly precise static terrestrial gravimetry, dynamic gravimetry facilitates the rapid coverage of large and remote regions. Satellite gravimetry enables the acquisition of gravity data on a global scale; however, due to the distance to the geoid, the spatial resolution is finite. Consequently, dynamic gravimetry has become a widely adopted approach in numerous applications, including regional geoid determination, geological research, exploration, and glaciology.

F. Johann (✉)
Physical and Satellite Geodesy, Technical University of Darmstadt, Darmstadt, Germany
e-mail: johann@psg.tu-darmstadt.de

H. Eisermann · G. Eagles
Alfred Wegener Institute for Polar and Marine Research, Bremerhaven, Germany
e-mail: hannes.eisermann@awi.de; graeme.eagles@awi.de

A. Ruppel
Federal Institute for Geosciences and Natural Resources (BGR), Hannover, Germany
e-mail: antonia.ruppel@bgr.de

International Association of Geodesy Symposia,
https://doi.org/10.1007/1345_2025_291,

Typically, a precision of gravity results between approximately 0.5 and 2 mGal (Studinger et al. 2008; Forsberg and Olesen 2010; Yuan et al. 2020; Johann 2023) (1 mGal = 10^{-5} m/s^2) is achievable after "end-matching" (Kwon and Jekeli 2001), i.e. by tying the results of relative gravity measurements to known terrestrial gravity values at the airfield/harbour between the flights/cruises. However, significant systematic errors can remain in the end-matched results due to sensor drifts of the gravimeters and possibly other unknown effects. These systematic deviations can be mitigated through levelling procedures, also referred to as "adjustment".

A straightforward and widely used levelling strategy is the crossover levelling. Assuming a static gravity field, the gravity residuals at obtained trajectory intersections, i.e. the "crossover points" (COs), are used to estimate drift parameters in a least-squares adjustment. A gravity bias can be estimated per flight/cruise or per approximately straight trajectory line (henceforth referred to as "line"). Thereby, the redundancy at the COs is used to enhance the precision of the gravity results. The seven campaigns described by Becker et al. (2016) and Johann et al. (2020) exhibit an average precision enhancement of 48%. When at least two COs are available per line, a linear drift can be estimated per line in addition to the line bias (Glennie and Schwarz 1999; Hwang et al. 2006; Zhang et al. 2017). In scenarios where the network contains a low number of COs, the risk of achieving overly optimistic precision values after adjustment can be reduced by incorporating correction factors into the crossover residuals at lines with few COs (Becker 2016). Nevertheless, in order to avoid a distortion of the resulting gravity network, a line-wise crossover levelling should only be applied if many COs per line are available. This outlines the primary limitation of crossover levelling: The adjusted results are dependent on a limited number of crossover residuals with the risk of result distortion. Hence, a reliable line-wise adjustment is only feasible for campaigns with a high number of COs per line; that is, many cross lines are required increasing the campaign duration and costs.

Instead of COs, the spatial neighbourhood of gravity observations can serve as input for gravity levelling, assuming similar low wavelength gravity at nearby points. For the levelling of magnetic field observations, various approaches based on directional filtering and (weighted) spatial median/average filters exist (Mauring and Kihle 2006; Ishihara 2015), as well as field modelling with subsequent line-wise drift estimation (White and Beamish 2015).

While the aforementioned approaches do not reflect the physical properties of the Earth's gravity field, Vyazmin (2020) uses strapdown gravimeter observations to estimate the sensor errors of the inertial measurement unit (IMU) simultaneously with the disturbance potential of the gravity field, modelled with spherical radial basis functions (SRBFs). The gravity disturbance is then computed as the gradient of the disturbance potential. A substantial limitation of this approach is that, since the resulting gravity disturbance is uniform at both adjacent lines at a CO, precision evaluation via crossover evaluation or repeated line analysis is not possible (Vyazmin et al. 2021). Li (2021) uses (unlevelled) airborne gravity disturbance data to estimate the gravity disturbance field (rather than the disturbance potential field). Within the same least-squares adjustment, he estimates gravity disturbance biases for each line. Like in the crossover levelling, the final gravity disturbance results are obtained by removing the estimated line biases from the unlevelled gravity disturbance. The computation of a precision indicator based on the adjusted crossover residuals is possible. The primary advantage of this method over CO levelling is that it uses the complete gravity disturbance trajectory for levelling. Hence, the method mitigates the risk of network distortion and avoids the necessity for a substantial number of crossing lines for levelling. Furthermore, a 2-D gravity disturbance field is estimated simultaneously within the least-squares adjustment.

This chapter presents the functional model of the CO and SRBF levelling approaches and their validation at the example of three airborne gravimetry campaigns with completely different trajectory designs. The existing levelling approaches are extended by estimating biases for equidistant trajectory segments instead of straight lines to allow for an application for campaigns with highly irregular trajectories. Section 2 presents the extended CO and SRBF levelling approaches. Section 3 introduces the three airborne gravimetry campaigns. The results of Sect. 3 are discussed in Sect. 4.

2 Methods

In this study, the levelling approaches are applied to results of gravity disturbance, i.e. the difference between gravity and normal gravity $\boldsymbol{\gamma}$, which are obtained with the direct method of strapdown gravimetry. This method is based on the subtraction of the 3-D accelerometer observations of an IMU, i.e. the so-called specific force $\boldsymbol{f}$, from the kinematic acceleration of the vehicle, yielding the gravity disturbance

$$\boldsymbol{\delta g}^i = \ddot{\boldsymbol{r}}^i - \boldsymbol{f}^i - \boldsymbol{\gamma}^i \tag{1}$$

in an inertial frame i. The kinematic acceleration is obtained as the second numerical derivative of the position, determined using Global Navigation Satellite Systems (GNSS). If the gravity disturbance is required to be expressed in a navigation frame, e.g. North, East, and Down, the specific force must be rotated from the body-fixed to the navigation frame. Additionally, the Eötvös correction considers (ficti-

tious) accelerations due to the rotating sensor frames. Details on the applied algorithm of the direct method of strapdown gravimetry can be found in the works of Johann et al. (2019) and Johann (2023). The commercial software NovAtel Waypoint Inertial Explorer is used for the GNSS positioning, applying a precise point positioning (PPP) approach with satellite correction data from the Centre for Orbit Determination in Europe (CODE) and for the GNSS/IMU integration to compute the vehicle orientation. The remaining calculations are performed with MATLAB software developed at the Technical University of Darmstadt (TUDa).

The CO and SRBF levelling approaches, where a bias is estimated per flight or line, are presented in detail in Sects. 2.1 and 2.2, respectively. Section 2.2 also outlines the advantages of modelling gravity field quantities using SRBFs. Section 2.3 introduces modifications to both levelling approaches that allow for the levelling of irregular flight trajectories.

2.1 Line-Wise CO Levelling

In the crossover levelling method used in this chapter, one bias is estimated per line. The model is based on Becker (2016) and Hwang et al. (2006). The residual $\chi_{A,B}$ at a CO with the observed gravity disturbances δg_A, δg_B at the adjacent lines A, B is the difference

$$\chi_{A,B} = \delta g_B - \delta g_A = \kappa_B - \kappa_A, \tag{2}$$

assuming error-free gravity disturbance except for the line biases κ_A, κ_B. Based on the linear functional model in Eq. (2), the line biases are estimated within a least-squares adjustment (Gauss-Markov model)

$$\boldsymbol{L} = \boldsymbol{A}\ \boldsymbol{X} + \boldsymbol{\varepsilon}, \quad \boldsymbol{X} = \left(\boldsymbol{A}^{\mathrm{T}}\boldsymbol{P}\boldsymbol{A}\right)^{-1}\boldsymbol{A}^{\mathrm{T}}\boldsymbol{P}\boldsymbol{L}, \tag{3}$$

with $\boldsymbol{L}$ being the observations, $\boldsymbol{A}$ being the design matrix, $\boldsymbol{X}$ being the parameters to be estimated, and $\boldsymbol{\varepsilon}$ being normally distributed random errors in the observations. Assuming uncorrelated observations with equal accuracy, the weight matrix $\boldsymbol{P}$ becomes the unit matrix. The observation vector contains the crossover residuals $\boldsymbol{\chi}$; the parameter vector contains the line biases as

$$\boldsymbol{L} = \begin{pmatrix} \boldsymbol{\chi} \\ 0 \end{pmatrix}_{(C+1)\times 1}, \quad \boldsymbol{X} = \boldsymbol{\kappa}_{M\times 1}, \tag{4}$$

with C, M being the number of COs and lines, respectively. A row of the complete design matrix

$$\boldsymbol{A}_{(C+1)\times M} = \left(\boldsymbol{A}_1^{\mathrm{T}}\ \boldsymbol{A}_2^{\mathrm{T}}\ \cdots\ \boldsymbol{A}_C^{\mathrm{T}}\ \boldsymbol{A}_{C+1}^{\mathrm{T}}\right)^{\mathrm{T}}, \tag{5}$$

corresponding to one CO j and the last row is obtained as

$$\boldsymbol{A}_j = \left(\boldsymbol{0}^{\mathrm{T}}\ {-1}\ \boldsymbol{0}^{\mathrm{T}}\ 1\ \boldsymbol{0}^{\mathrm{T}}\right)_{1\times M}, \quad \boldsymbol{A}_{C+1} = \boldsymbol{1}^{\mathrm{T}}. \tag{6}$$

The columns of -1 and 1 correspond to the indices of the adjacent lines of the CO. The last row avoids a rank defect by introducing the pseudo-observation that the sum of all line biases is zero.

2.2 Line-Wise SRBF Levelling

The approach of the SRBF-based levelling is based on Li (2021) and is executed after the computation of the unlevelled gravity disturbance. The gravity disturbance results of a global gravity model evaluated up to degree and order $N_{\min}$ may be subtracted from the gravity disturbance before SRBF levelling. For an epoch i and a line l, the gravity disturbance portion in the bandwidth between the orders $N_{\min}$, $N_{\max}$ is assumed to be

$$\delta g_{i,l} = \kappa_l + \delta g_{\mathrm{mod},i} = \kappa_l + \frac{GM}{R^2}\sum_{k=1}^{K}\alpha_k B_{i,k}, \tag{7}$$

i.e. the sum of the line bias κ_l, and an SRBF-based regional gravity disturbance model $\delta g_{\mathrm{mod},i}$. GM is the geocentric gravitational constant, R is the Earth's mean radius under spherical approximation, $B_{i,k}$ is an SRBF with a scaling factor α_k, and K is the total number of SRBFs. An SRBF is obtained as

$$B_{i,k} = \sum_{n=N_{\min}}^{N_{\max}} b_n \left(\frac{R}{r_i}\right)^{n+2} (n+1)\sqrt{2n+1}\ \overline{P}_n\left(\cos\psi_{i,k}\right). \tag{8}$$

As kernel b_n, the Shannon kernel $b_n = 1$ is used in this study. For details on kernel types, see Bentel et al. (2013) and Lieb et al. (2016). r_i is approximated as $r_i = R + h_i$, with h_i being the ellipsoidal height. The weighting based on the spherical distance

$$\psi_{i,k} = \overline{\boldsymbol{r}}_i^{\mathrm{T}}\overline{\boldsymbol{r}}_k, \tag{9}$$

with $\overline{\boldsymbol{r}}_i, \overline{\boldsymbol{r}}_k$ being the normed Cartesian geocentric coordinates, i.e. unit vectors, of the δg observation point i and the SRBF origin k, respectively (Klees et al. 2008), is computed using normed Legendre polynomials $\overline{P}_n$ (see e.g. Torge et al. 2023) for a degree n. If the factors in Eq. (8) would be adapted, other functionals of the gravity field like the potential or gradient could be estimated instead of the gravity disturbance field (Liu et al. 2020).

In a least-squares adjustment according to Eq. (3), Eq. (7) serves as linear observation equation, i.e. the obtained gravity disturbances δg_i for N epochs i along the trajectory are the observations, and the scaling factors α_k of the SRBFs k are estimated along with the line biases κ_l,

$$\boldsymbol{L} = \begin{pmatrix} \boldsymbol{\delta g} \\ 0 \end{pmatrix}_{(N+1)\times 1}, \quad \boldsymbol{X} = \begin{pmatrix} \boldsymbol{\alpha} \\ \boldsymbol{\kappa} \end{pmatrix}_{(K+M)\times 1}. \tag{10}$$

The design matrix is set up as

$$\begin{aligned} &\boldsymbol{A}_{(N+1)\times(K+M)} = \left(\boldsymbol{A}_1^{\mathrm{T}}\ \boldsymbol{A}_2^{\mathrm{T}} \cdots \boldsymbol{A}_N^{\mathrm{T}}\ \boldsymbol{A}_{N+1}^{\mathrm{T}}\right)^{\mathrm{T}}, \quad \text{with} \\ &\boldsymbol{A}_i = \left(\tfrac{GM}{R^2}\boldsymbol{B}_{i,1} \cdots \tfrac{GM}{R^2}\boldsymbol{B}_{i,k}\ \boldsymbol{A}_{i,\mathrm{end}}\right)_{1\times(K+M)}, \\ &\boldsymbol{A}_{i,\mathrm{end}} = \left(\mathbf{0}^{\mathrm{T}}\ 1\ \mathbf{0}^{\mathrm{T}}\right), \quad \boldsymbol{A}_{N+1} = \left(\mathbf{0}_{1\times K}\ \mathbf{0}_{1\times M}\right), \end{aligned} \tag{11}$$

where the last row introduces the same pseudo-observation like in Eq. (6). The column of 1 in $\boldsymbol{A}_i$ corresponds to the index of the current line in the parameter vector in Eq. (10).

The quality of the gravity field parameters estimated in SRBF levelling strongly depends on the selection of some processing parameters, such as the kernel functions (Bentel et al. 2013; Lieb et al. 2016), the distribution and number of SRBFs (Klees et al. 2008; Bentel et al. 2013; Lieb et al. 2016), the subsampling and ratio of the gravity disturbance observations in comparison to the number of SRBFs (Klees et al. 2008; Li 2018), and the SRBF bandwidth (Klees et al. 2008; Lieb et al. 2016). For details on an appropriate parameter selection, the reader is referred to the mentioned references. However, due to the large number of possibilities and combinations, some trial and error is required to find optimal results for modelling the gravity (disturbance) field in a particular campaign or target region (Ma 2024). It has been found that the computation area, i.e. the area covered by SRBF origins, needs to be larger than the observation area, and the latter should be larger than the target area, because the result quality decreases near the outer observation boundary (Bentel et al. 2013; Lieb et al. 2016; Liu et al. 2024).

2.3 Modification: Segment-Wise Levelling

The dependence on flight lines in the levelling methods introduced in Sects. 2.1 and 2.2 has drawbacks. Typically, the duration of the lines varies, and they are not evenly distributed throughout a flight. When parts of a flight or even the whole flight do not have straight lines, they cannot be levelled with the traditional line-based methods. This chapter introduces a new type of levelling that divides the flights into equidistant segments that are independent of possibly irregular lines (Fig. 1). Instead of estimating a bias per line, biases are estimated in-between of the segments. The number

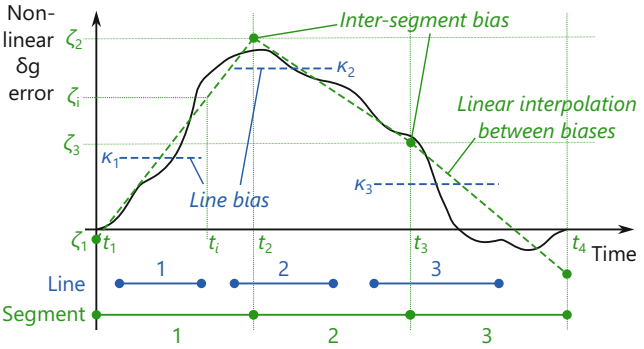

Fig. 1 Line-wise (blue) and segment-wise (green) levelling methods on the example of a non-linear gravity disturbance error during a fictitious flight with three lines, divided into three segments. In the line-wise levelling type, the error is approximated by a bias that is estimated for each approximately straight flight line, omitting trajectory parts between the lines. In the segment-wise levelling type, the trajectory is divided into equidistant segments, and the error is interpolated between biases before and after each segment

of segments can be selected by the user based on the expected non-linear variation of the gravity disturbance error.

The gravity disturbance error

$$\begin{aligned} \zeta_i &= \zeta_1 + (\zeta_2 - \zeta_1)\,\frac{t_i - t_1}{T} = (1 - p_i)\ \zeta_1 + p_i \zeta_2, \\ &\text{with} \quad p_i := \frac{t_i - t_1}{T} = \frac{t_i - t_1}{t_2 - t_1}, \end{aligned} \tag{12}$$

at an epoch t_i of segment 1 is obtained by interpolation between the previous and subsequent biases ζ_1, ζ_2 at the epochs t_1, t_2 at the beginning and end of the line. The segment duration T is equal for all segments.

For the segment-wise type, the residual at a CO becomes

$$\begin{aligned} \chi_{A,B} &= \delta g_B - \delta g_A = \zeta_B - \zeta_A \\ &= (1 - p_B)\,\zeta_{B,1} + p_B \zeta_{B,2} + (p_A - 1)\,\zeta_{A,1} - p_A \zeta_{A,2} \end{aligned} \tag{13}$$

by replacing the line biases κ_A, κ_B in Eq. (2) by the gravity disturbance errors ζ_A, ζ_B of Eq. (12), which are interpolated between the neighbouring inter-segment biases $\zeta_{A,1}$, $\zeta_{A,2}$, $\zeta_{B,1}$, $\zeta_{B,2}$. The indices A, B represent both adjacent trajectory segments at the CO; the indices 1, 2 represent the beginning and end of the particular segment. While the observations $\boldsymbol{L}$ remain unchanged compared to Eq. (4), the parameter vector becomes $\boldsymbol{X} = \boldsymbol{\zeta}_{(S+1)\times 1}$. Since one bias is estimated before and after each segment, the length of $\boldsymbol{X}$ is the number of segments S plus one. To enable a least-squares adjustment according to Eq. (3), the design matrix is set up like in Eq. (5), with $S + 1$ columns, but a row j of the design matrix becomes

$$\boldsymbol{A}_j = \left(\mathbf{0}^{\mathrm{T}}\ \ p_A - 1\ \ -p_A\ \mathbf{0}^{\mathrm{T}}\ \ 1 - p_B\ \ p_B\ \ \mathbf{0}^{\mathrm{T}}\right)_{1\times M}, \tag{14}$$

translated from Eq. (13). The indices of the non-zero columns correspond to the indices of the parameters $\zeta_{A,1}$, $\zeta_{A,2}$, $\zeta_{B,1}$, $\zeta_{B,2}$. The last row consists of ones, like in Eq. (6).

The segment-wise type can also be applied to the SRBF levelling. The observation equation then becomes

$$\delta g_{i,s} = (1 - p_i)\,\zeta_{s,1} + p_i\,\zeta_{s,2} + \delta g_{\mathrm{mod},i}\,, \tag{15}$$

where, in comparison to Eq. (7) of the CO levelling, the line bias κ_l is replaced by the gravity disturbance error of Eq. (12), with $\zeta_{s,1}$, $\zeta_{s,2}$ being the neighbouring biases at the beginning and the end of the current segment s. The observation vector $\boldsymbol{L}$ remains unchanged compared to Eq. (10); the parameter vector becomes $\boldsymbol{X} = \left(\boldsymbol{\alpha}^{\mathrm{T}}\ \boldsymbol{\zeta}^{\mathrm{T}}\right)^{\mathrm{T}}_{(K+S+1)\times 1}$. The design matrix of Eq. (11) is modified according to Eq. (13) as

$$\begin{aligned}
&\boldsymbol{A}_{(N+1)\times(K+S+1)} = \left(\boldsymbol{A}_1^{\mathrm{T}}\ \boldsymbol{A}_2^{\mathrm{T}} \cdots \boldsymbol{A}_N^{\mathrm{T}}\ \boldsymbol{A}_{N+1}^{\mathrm{T}}\right)^{\mathrm{T}}, \quad \text{with}\\
&\boldsymbol{A}_i = \left(\tfrac{GM}{R^2} B_{i,1} \cdots \tfrac{GM}{R^2} B_{i,k}\ \boldsymbol{A}_{i,\mathrm{end}}\right)_{1\times(K+S+1)},\\
&\boldsymbol{A}_{i,\mathrm{end}} = \left(\boldsymbol{0}^{\mathrm{T}}\ 1 - p_i\ p_i\ \boldsymbol{0}^{\mathrm{T}}\right),\\
&\boldsymbol{A}_{C+1} = \left(\boldsymbol{0}_{1\times K}\ \boldsymbol{1}_{1\times(S+1)}\right).
\end{aligned} \tag{16}$$

3 Validation in Dynamic Campaigns

The line- and segment-wise CO and SRBF levelling methods introduced in Sect. 2 were applied to the gravity disturbance results of three airborne campaigns. The Odenwald 2018 campaign ("ODW2018") and its results are presented in Sect. 3.1. With a dense line network and significant errors in the unlevelled gravity disturbance, ODW2018 is well suited for CO and SRBF levelling. The RIISERBATHY/GEA-VI campaign ("GEA-VI"), which is presented in Sect. 3.2, includes different areas with varying line network density. The trajectory of the CASE 23-Aerogeophysics ("CASE 23") campaign lacks straight lines and has a very low number of COs. It is therefore a good example for testing the segment-wise SRBF levelling method. The main characteristics and SRBF settings of all three campaigns are summarised in Table 1.

In all campaigns, the iMAR iNAV-RQH-1003 (iMAR Navigation 2012; Johann 2023) owned by TUDa was used as strapdown gravimeter. In the GEA-VI and CASE 23 campaigns, it was additionally equipped with a temperature-stabilising housing, the iTempStab-AddOn. In the SRBF levelling, the SRBF origins were homogeneously distributed based on Reuter grids (Eicker 2008). The other SRBF modelling settings, including the origin separation, the buffer radius defining the area covered by the origins, and the minimal and maximal model degrees in Eq. (8), were selected for the campaigns individually as stated in Table 1, depending on the covered area, the flight velocity and altitude, and the variability of the gravity disturbance field. If the lower wavelengths of a global gravitational model were subtracted from the unlevelled gravity disturbance, the EGM2008 (Pavlis et al. 2012) was used. While the choice of the above SRBF settings required careful tuning, the addition and choice of a global model were found to lead to only small result changes. Table 2 shows the crossover precision based on the root mean square error (RMSE), which is obtained by dividing the RMS of the residuals at the COs by $\sqrt{2}$. CO residuals with height differences of both adjacent trajectories of more than 150 m were removed from the computation to ensure comparability of the precision indicators between different campaigns. The number of segments was selected in a process optimising the CO RMSE. The optimal number of segments decreases with a decreasing non-linear gravity disturbance error variation.

Table 1 Campaign characteristics (upper part) and SRBF settings (lower part) (ODW2018 data based on Johann et al. (2020))

Properties/settings	ODW2018	GEA-VI	CASE 23
Mean ellipsoidal height [m]	947	1,005	486
Mean velocity [m/s]	54	76	47
Turbulence (RMS-g) [mm/s^2]	128	240	608
Filter length (−6 dB) [s]	120	130	160
Half-wave. resolution [km]	3.3	4.9	3.7
Variability $\lvert\dot{\delta g}\rvert$ [mGal/km]	2.7	1.6	2.1
Number of COs	222	184	32
Segments per flight	55	2	1
SRBF separation [km]	7.5	50	20
SRBF buffer [km]	20	360	60
SRBF degree range	400–2,400	200–800	450–850
Global model subtracted	No	Yes	Yes

Table 2 Crossover point RMSE (all values in mGal)

Levelling	ODW2018		GEA-VI		CASE 23	
	CO	SRBF	CO	SRBF	CO	SRBF
None	4.05		1.71		2.16	
Line-wise	0.64	0.63	1.01	1.53	–	–
Segment-wise	0.53	0.83	1.02	1.24	–	2.08

3.1 Dense Regular Grid: Odenwald 2018

In March 2018, a test flight (ODW2018) was conducted with a light aircraft Cessna 206 "Stationair 6" at the low mountain range Odenwald near Frankfurt, Germany. Details on the campaign are presented by Johann et al. (2020) and Johann (2023). The presence of strong non-linear drifts in the unlevelled gravity disturbance results (Fig. 2) and the high CO RMSE of 4.05 mGal are attributed to environmental temperatures close to the freezing point in the morning and lack of temperature stabilisation. However, the large number of COs per line permits a robust line bias estimation in the

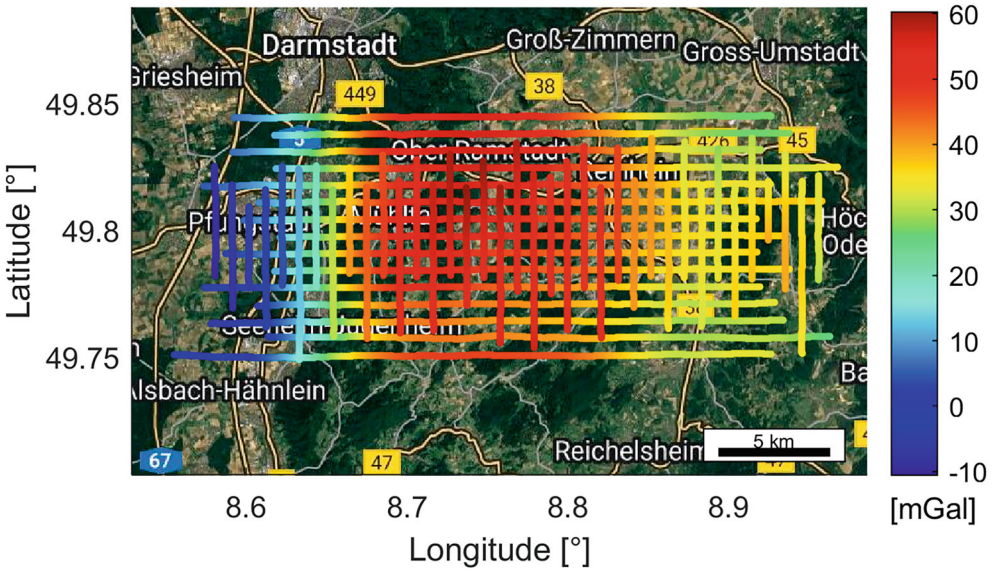

Fig. 2 Gravity disturbance [mGal] along the lines of ODW2018 before levelling (map data: Google, Landsat/Copernicus)

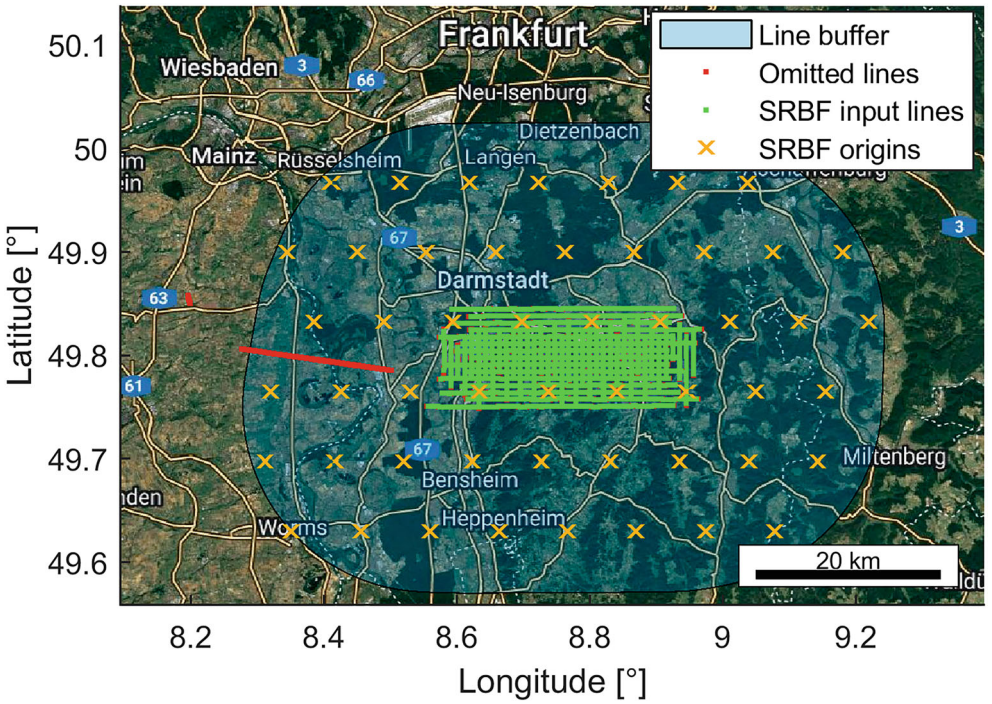

Fig. 3 ODW2018 lines and SRBF origins within a buffer area (map data: Google, Landsat/Copernicus)

CO levelling, resulting in a strongly improved RMSE of 0.64 mGal (see Table 2). When the novel segment-wise CO adjustment (see Sect. 2.3) is applied, dividing the flight into 55 segments, the RMSE further improves to 0.53 mGal.

Figure 3 depicts the distribution of the SRBF origins in and around the survey area. All Reuter grid positions located beyond a buffer area surrounding the flight lines were omitted. Isolated lines west of the grid were removed beforehand. After line-wise SRBF levelling, the precision is on par with CO levelling (see Table 2). The estimated line biases are illustrated in Fig. 4. While the obtained biases are very similar, the SRBF method allows for the estimation of additional outer lines with an insufficient number of CO for CO adjustment. For the segment-wise type, the CO levelling outperforms the SRBF levelling (see Table 2).

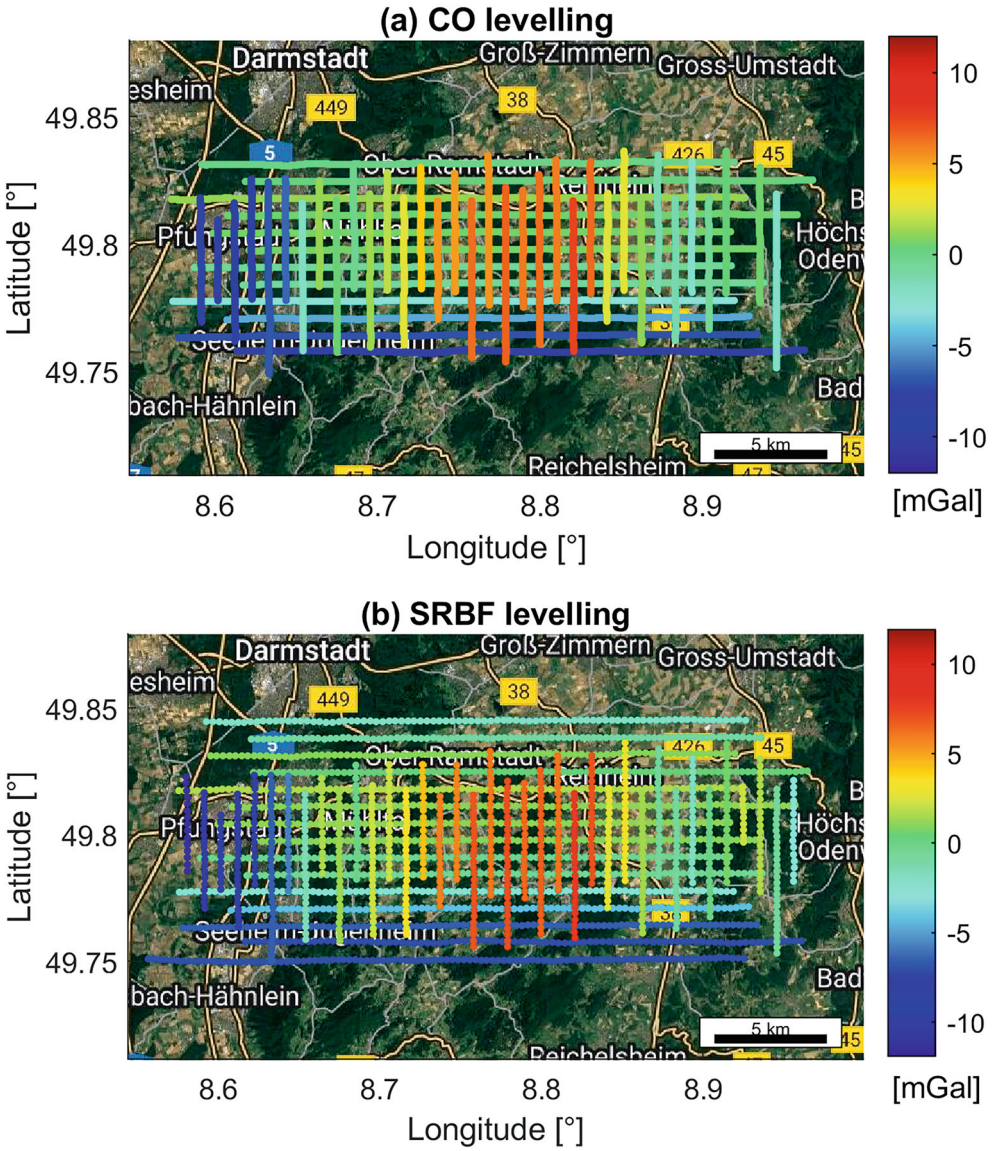

Fig. 4 Estimated line biases [mGal] of ODW2018 (map data: Google, Landsat/Copernicus): (**a**) CO levelling; (**b**) SRBF levelling

3.2 Large Polar Grid: RIISERBATHY/GEA-VI 2022/23

In the Antarctic summer of 2022/23, the Alfred Wegener Institute for Polar and Marine Research (AWI) and the Federal Institute for Geosciences and Natural Resources (BGR) conducted an airborne campaign, designated RIISERBATHY/GEA-VI (GEA-VI), at the Riiser-Larsen Ice Shelf, East Antarctica. Based at the Neumayer III station in the Northeast, ten survey flights were conducted with a Basler BT-67, resulting in a dense trajectory net in the Northeast and lines widening towards the Southeast (Fig. 5). Details on the campaign and a comparison of the strapdown gravimeter to an additionally installed stable-platform gravimeter can be found in the work of Johann et al. (2025a). The strapdown results are available in the study of Johann et al. (2025b). Without levelling, the CO RMSE is 1.71 mGal. After line-wise CO levelling, the RMSE becomes 1.01 mGal (see Table 2). Given the negligible line-to-line drift observed in this campaign (Johann et al. 2025a), the segment-wise CO levelling performs best (1.02 mGal) when only two segments per flight are used.

Applying line-wise SRBF levelling results in a reduction of formerly large CO residuals in the dense trajectory area in the Northeast, while CO residuals at the wider line spacing in the Southwest generally increase (Fig. 6a, b). The RMSE slightly improves to 1.53 mGal. The segment-wise SRBF levelling performs better over the complete survey area (Fig. 6c), resulting in an RMSE of 1.24 mGal.

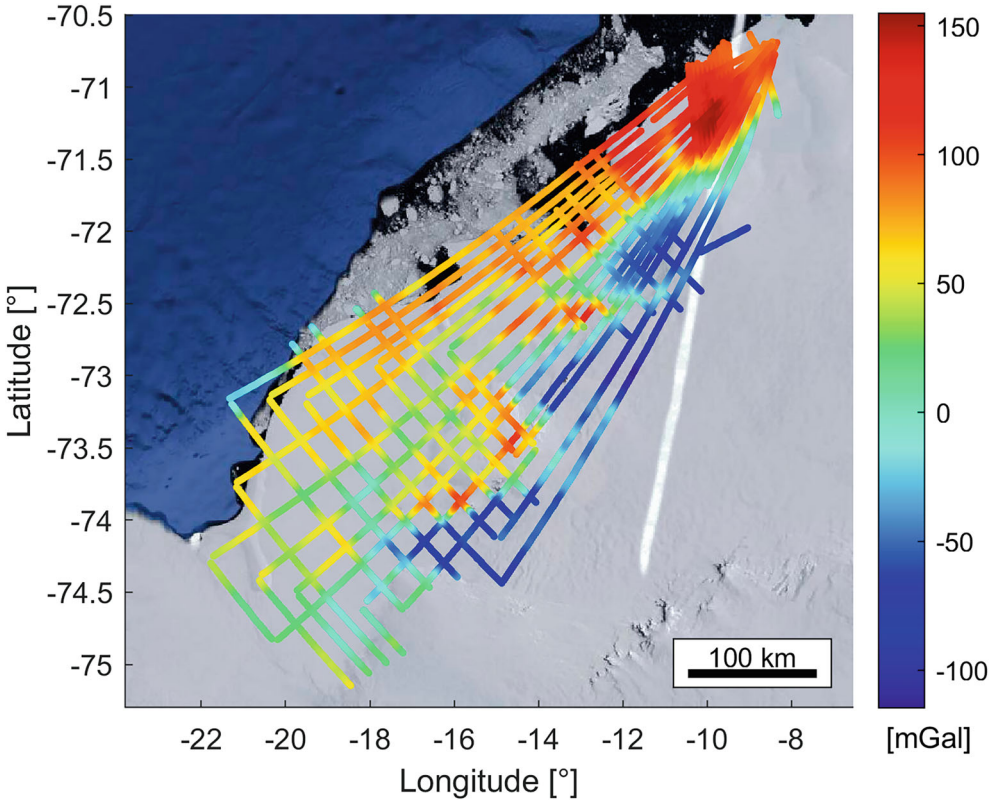

Fig. 5 Gravity disturbance [mGal] along the lines of GEA-VI before levelling (map data: Google, U.S. Geological Survey)

3.3 Irregular Trajectory: CASE 23-Aerogeophysics

While the aforementioned campaigns used fixed-wing aircraft, a helicopter (Airbus H125) was deployed during the expedition CASE 23-Aerogeophysics (CASE 23) in August 2023 across Nordenskiöld Land, Svalbard, led by the BGR. Like at GEA-VI, the gravimeter was equipped with temperature stabilisation and was turned on also between the flights to minimise the influence of thermally induced drifts. Due to unfavourable weather conditions, all four flights followed the valleys of Nordenskiöld Land instead of flying along straight flight lines (Fig. 7); the flight altitude followed the terrain height. After the removal of only the narrowest turns from the results, 32 COs remained, with an RMSE of 2.16 mGal. Due to the lack of straight lines and with the low number of COs, line-wise levelling and CO levelling were not possible (see Table 2). Consequently, the sole viable levelling method was the segment-wise SRBF levelling, which resulted in a slightly improved RMSE of 2.08 mGal when two biases were estimated per flight. The magnitude of the interpolated bias was low (Fig. 8), particularly when contrasted to the ODW2018 campaign that did not incorporate temperature stabilisation (see Fig. 4).

4 Discussion

The application of the levelling methods introduced in Sect. 2 to three airborne campaigns with very different trajectory layouts and local gravity fields unveils differing properties of the methods. The ODW2018 flight comprises almost ideal conditions for all levelling methods because it features a dense line network with many COs per line and levelling has a large improvement potential due to the large thermally induced gravity disturbance errors. All methods lead to strong improvements (see Table 2). The good performance of the segment-wise CO levelling suggests that the error in the un-levelled results is not line dependent.

The disparity in the enhancement of CO residuals across the Northeast and Southwest regions of GEA-VI indicates that the selection of SRBF settings like the SRBF origin distribution and spacing may not be equally well suited to trajectory parts with dense and wide line spacing. For the irregular trajectory of CASE 23 with rapid altitude changes, attributable to the terrain following flight mode, an RMSE for the unlevelled results of 2.16 mGal is deemed satisfactory. The SRBF levelling is the only method applicable to this challenging trajectory with a low number of COs.

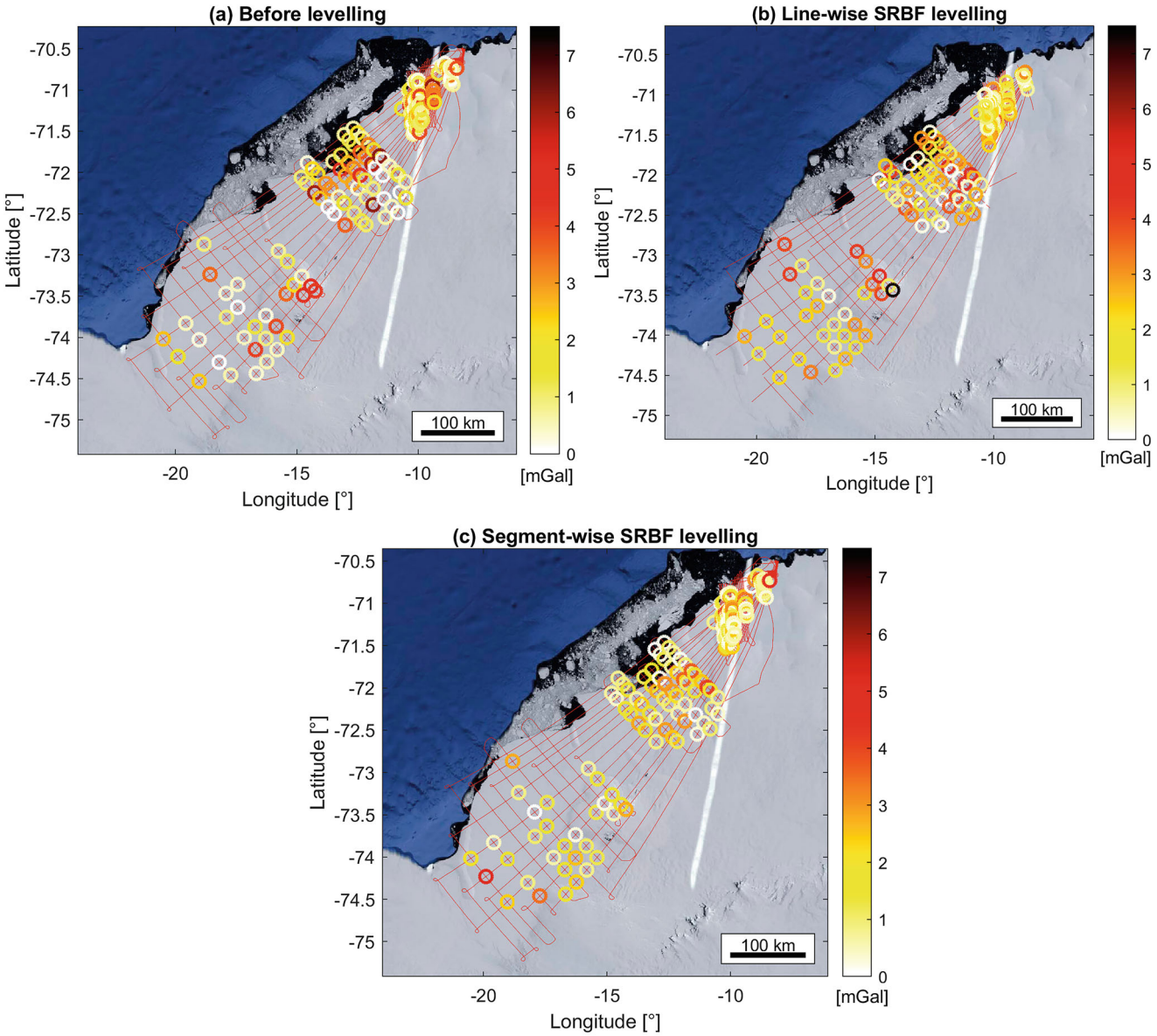

Fig. 6 Crossover point residuals [mGal] at GEA-VI (map data: Google, U.S. Geological Survey): (**a**) before levelling; (**b**) line-wise SRBF levelling; (**c**) segment-wise SRBF levelling

5 Conclusions and Outlook

CO and SRBF levelling methods were presented and evaluated. Biases were estimated for each flight line, which is the default approach in gravimetry, and, alternatively, between equidistant trajectory segments, which is a newly introduced approach. All levelling methods were shown to improve a CO RMSE from 4.05 mGal to values ranging between 0.53 and 0.83 mGal. In most cases, the CO levelling performed slightly better than the SRBF levelling. However, the SRBF method uses the gravity disturbance along the entire trajectory instead of being restricted to a few CO residuals. Hence, it was shown to enable bias estimation even for lines without COs. The new segment-wise SRBF method was shown to be capable of slight improvements in a campaign with a heterogeneous trajectory and a very low number of crossover points where a classical line-wise CO levelling could not have been applied.

In subsequent studies, the implementation of a topographic reduction prior to SRBF levelling may be considered to distinguish between sensor errors and gravity variations induced by the topography. Especially in campaigns with a high field variability and broad line spacing, enhancements in the SRBF levelling results are expected. In campaigns with a varying line spacing, a more sophisticated SRBF origin

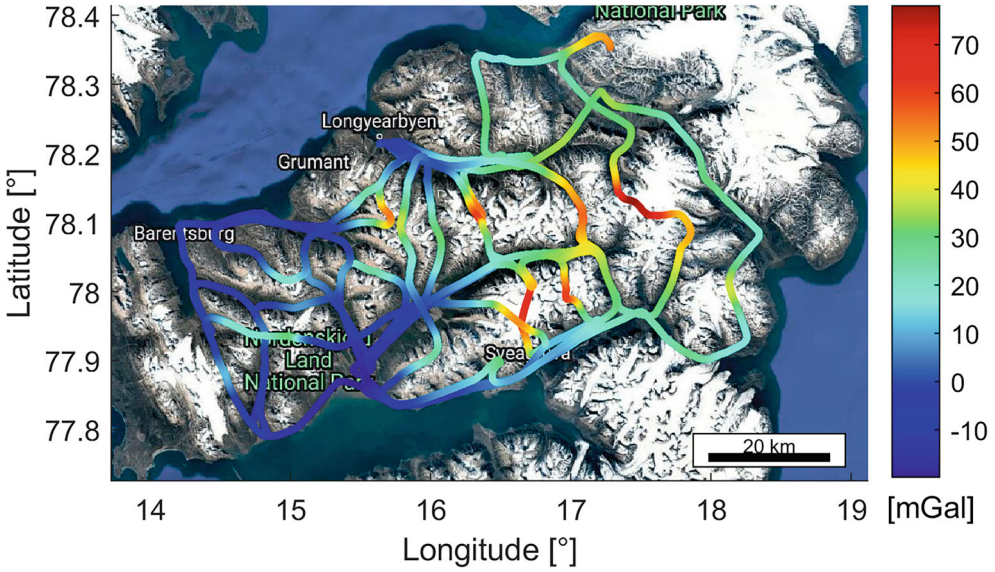

Fig. 7 Gravity disturbance [mGal] along the complete trajectory of CASE 23 before levelling (map data: Google, Landsat/Copernicus)

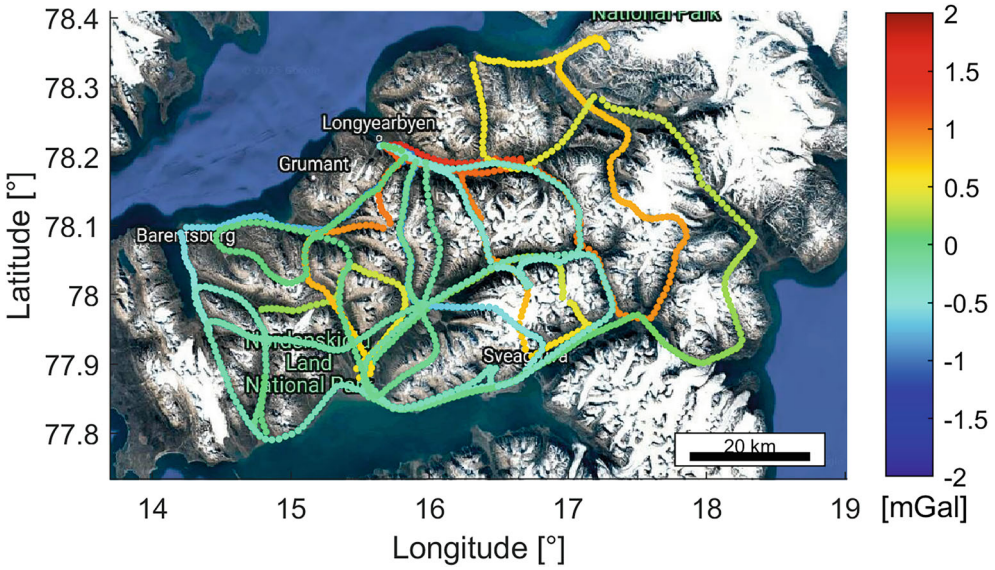

Fig. 8 Interpolated inter-segment biases [mGal] from SRBF levelling along the trajectory of CASE 23 (map data: Google, Landsat/Copernicus)

distribution, e.g. with more origins close to the trajectory (Klees et al. 2008), may prove advantageous. A comprehensive investigation into the impact of SRBF settings on the gravity disturbance results may also be recommended.

Acknowledgements The Odenwald 2017 campaign was conducted by TUDa in cooperation with DTU Space, the Technical University of Dresden, and the Technical University of Munich. The RIISERBATHY/GEA-VI campaign 2022/23 was conducted by the Alfred Wegener Institute for Polar and Marine Research (AWI) and the German Federal Institute for Geosciences and Natural Resources (BGR) in cooperation with TUDa. The CASE 23-Aerogeophysics campaign was organised by the BGR as part of CASE 23, with a cooperation with TUDa for the airborne project. H. Eisermann is funded through the INSPIRES program at the Alfred Wegener Institute.

References

Becker D (2016) Advanced calibration methods for strapdown airborne gravimetry. Technische Universität Darmstadt

Becker D, Becker M, Olesen AV, Nielsen JE, Forsberg R (2016) Latest results in strapdown airborne gravimetry using an iMAR RQH unit. In: 4th IAG symposium on terrestrial gravimetry. State Research Center of the Russian Federation, pp 19–25

Bentel K, Schmidt M, Rolstad Denby C (2013) Artifacts in regional gravity representations with spherical radial basis functions. J Geod Sci 3(3):173–187. https://doi.org/10.2478/jogs-2013-0029

Eicker A (2008) Gravity field refinement by radial basis functions from in-situ satellite data. Universität Bonn

Forsberg R, Olesen AV (2010) Airborne gravity field determination. In: Xu G (ed) Sciences of geodesy-I: advances and future directions. Springer, Berlin, pp 83–104

Glennie CL, Schwarz KP (1999) A comparison and analysis of airborne gravimetry results from two strapdown inertial/DGPS systems. J Geod 73:311–321. https://doi.org/10.1007/s001900050248

Hwang C, Hsiao YS, Shih HC (2006) Data reduction in scalar airborne gravimetry: theory, software and case study in Taiwan. Comput Geosci 32:1573–1584. https://doi.org/10.1016/j.cageo.2006.02.015

IMAR Navigation (2012) iNAV-RQH-1003: inertial measurement system for advanced applications. https://www.imar-navigation.de/downloads/NAV_RQH_1003_en.pdf. Accessed 17 May 2024

Ishihara T (2015) A new leveling method without the direct use of crossover data and its application in marine magnetic surveys: weighted spatial averaging and temporal filtering. Earth Planets Space 67(1):1–14. https://doi.org/10.1186/s40623-015-0181-7

Johann F (2023) Magnetic calibration and GNSS processing in strapdown dynamic gravimetry. Technical University of Darmstadt

Johann F, Becker D, Becker M, Forsberg R, Kadir M (2019) The direct method in strapdown airborne gravimetry – a review. Z Geod Geoinf Land Manag 144(5):323–333. https://doi.org/10.12902/zfv-0263-2019

Johann F, Becker D, Becker M, Ince ES (2020) Multi-scenario evaluation of the direct method in strapdown airborne and shipborne gravimetry. In: International Association of Geodesy symposia. Springer, Berlin, pp 1–8

Johann F, Eisermann H, Eagles G (2025a) A comparison and combination of stable platform and strapdown airborne gravimeters. J Appl Geophys 241:1–12. https://doi.org/10.1016/j.jappgeo.2025.105826

Johann F, Eisermann H, Eagles G (2025b) Airborne strapdown gravity disturbance data (iNAV) across Riiser-Larsen Ice Shelf, East Antarctica, from 2022/23 (RIISERBATHY Project) [dataset]. PANGAEA. https://doi.org/10.1594/PANGAEA.974371

Klees R, Tenzer R, Prutkin I, Wittwer T (2008) A data-driven approach to local gravity field modelling using spherical radial basis functions. J Geod 82(8):457–471. https://doi.org/10.1007/s00190-007-0196-3

Kwon JH, Jekeli C (2001) A new approach for airborne vector gravimetry using GPS/INS. J Geod 74:690–700. https://doi.org/10.1007/s001900000130

Li X (2018) Using radial basis functions in airborne gravimetry for local geoid improvement. J Geod 92(5):471–485. https://doi.org/10.1007/s00190-017-1074-2

Li X (2021) Leveling airborne and surface gravity surveys. Appl Geomat 13(4):945–951. https://doi.org/10.1007/s12518-021-00402-2

Lieb V, Schmidt M, Dettmering D, Börger K (2016) Combination of various observation techniques for regional modeling of the gravity field. J Geophys Res Solid Earth 121(5):3825–3845. https://doi.org/10.1002/2015JB012586

Liu Q, Schmidt M, Pail R, Willberg M (2020) Determination of the regularization parameter to combine heterogeneous observations in regional gravity field modeling. Remote Sens 12(10):1–25. https://doi.org/10.3390/rs12101617

Liu Q, Schmidt M, Sánchez L, Moisés L, Cortez D (2024) High-resolution regional gravity field modeling in data-challenging regions for the realization of geopotential-based height systems. Earth Planets Space 76(1):1–24. https://doi.org/10.1186/s40623-024-01981-1

Ma Z (2024) Gravity field modeling in mountainous areas based on band-limited SRBFs. J Geod 98(5). https://doi.org/10.1007/s00190-024-01852-3

Mauring E, Kihle O (2006) Leveling aerogeophysical data using a moving differential median filter. Geophysics 71(1):5–12. https://doi.org/10.1190/1.2163912

Pavlis NK, Holmes SA, Kenyon SC, Factor JK (2012) The development and evaluation of the Earth Gravitational Model 2008 (EGM2008). J Geophys Res Solid Earth 117(4):1–38. https://doi.org/10.1029/2011JB008916

Studinger M, Bell R, Frearson N (2008) Comparison of AIRGrav and GT-1A airborne gravimeters for research applications. Geophysics 73(6). https://doi.org/10.1190/1.2969664

Torge W, Müller J, Pail R (2023) Geodesy, 5th edn. De Gruyter Oldenbourg, Berlin, Boston

Vyazmin VS (2020) New algorithm for gravity vector estimation from airborne data using spherical scaling functions. https://doi.org/10.1007/1345_2020_113

Vyazmin V, Golovan A, Bolotin Y (2021) New strapdown airborne gravimetry algorithms: testing with real flight data. In: 28th Saint Petersbg international conference on integrated navigation systems (ICINS 2021). https://doi.org/10.23919/icins43216.2021.9470826

White JC, Beamish D (2015) Levelling aeromagnetic survey data without the need for tie-lines. Geophys Prospect 63(2):451–460. https://doi.org/10.1111/1365-2478.12198

Yuan Y, Gao J, Wu Z, Shen Z, Wu G (2020) Performance estimate of some prototypes of inertial platform and strapdown marine gravimeters. Earth Planets Space 72(1). https://doi.org/10.1186/s40623-020-01219-w

Zhang X, Zheng K, Lu C, Wan J, Liu Z, Ren X (2017) Acceleration estimation using a single GPS receiver for airborne scalar gravimetry. Adv Space Res 60:2277–2288. https://doi.org/10.1016/j.asr.2017.08.038